AKUSTIKA

**Volume 44
October/Říjen
2022**

Riemannian Matched Field Processing
Monography

Riemannian Matched Field Processing
Monograph

Tran Cao Quyen

Preface

As far as underwater source localization is concerned the Matched Field Processing (MFP) is an effective method. Floating ship localization, submarine localization in military section and fish finding in civilization are considered as the main application of MFP. Besides, determining environmental parameters such as sound speed profile, bottom topography and array tilt are also developed.

Some methods such as empirical mode decomposition, adaptive MFP, compressive MFP and especially stochastic MFP using Riemannian geometry (RMFP) have been introduced recently in order to increase MFP's reliability and resolution. It seems that the RMFP is the strongest candidate for the future development of MFP since it is inherited the strong foundation of both MFP and Riemannian Geometry. Surprisingly, not only the nature of curvature of sound wave but also the nature of MFP are exploited in RMFP.

The aim of this monograph is introduce RMFP by considering the Riemannian distance instead of Euclidean distance. Two approaches of RMFP construction, i.e., iso-metric mappings and direct Riemannian distance calculation are introduced.

The organization of this monograph is as follows. Two first chapters of this monograph revised the reader about the essential meaning of Gauss Curvature, Geodesic equation, iso-metric mapping in Riemannian Geometry and the state of the art of MFP. Chapter 3 presents Riemannian MFP. Chapter 4 concludes the monograph with discussions about the performance of MFP.

This monograph is designed for graduated students, scientists and senior engineers who working in the field of underwater acoustic engineering.

CONTENT

CHAPTER 1.

GAUSS THEOREM

Fig. 1. 1 Maximum line curvature in space

The purpose of this chapter is provide the concept of line curvature in space, Gauss curvature and their quantities in view of differential geometry. In this chapter, the principles of forming the Geodesic equation and the iso-metric mapping in Riemannian Geometry are also introduced.

1. 1.   Line curve in space

The continuous curve parameterization [1–2] in R^n (n=2,3,..) is a continuous function , in $\gamma : I \to R^n$ which $I \subset R$ is an open interval with their limits $-\infty \leq a < b \leq \infty$
Given the point P on the curve, the tangent vector at the point P is given by

$$\gamma_P^{'} = \frac{d\gamma}{ds}\bigg|_{s=P} \qquad (1.1)$$

Given γ as continuous curve parameterization the line curvature at the point P in space is the rate of change of tangent vector at the point P.

The line curvature at the point P is given by [1–2]

$$K(p) = \frac{\left\| \gamma_P^{'} \times \gamma_P^{''} \right\|}{\left\| \gamma_P^{'} \right\|^3} \qquad (1.2)$$

Where $\gamma_P^{''}$ is the second derivative of γ at the point P. To justify the $K(p)$ is not difficult for the reader.

Fig. 1. 1 illustrate the line curvature concept when comparing the line curvature with the maximum curvature possible, i.e., the curvature of a circular ($K(p)$=1/r with r is the radius of the circular).

1. 2.   The first fundamental form

The continuous parameterization of a surface in R^3 is a continuous function $x : U \to R^3$ with $U \subset R^2$ is non empty open set.
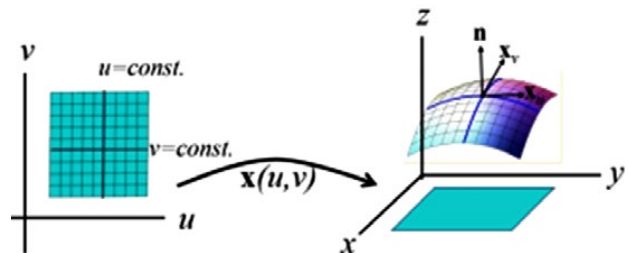
Fig. 1. 2 The parameterization of a surface

For example, consider the point P with coordinate x(u,v). The image of P is point P' in S=x(U) in new coordinate chart. Since x is not injection so there is a possibility of more than one coordinate of P' in its image.

Given the surface parameterization and coordinate chart x, the tangent vectors which are forming the tangent space at the point P can be written as

$$x_u = dx / du; x_v = dx / dv \qquad (1.3)$$

Assume that the tangent vector, $\mathbf{w}$, at the point P with coordinate a and b so

$$\omega = ax_u + bx_v \qquad (1.4)$$

The first fundamental form is given by [1–6]

$$I = \langle \mathbf{w},\mathbf{w} \rangle = \langle ax_u + bx_v, ax_u + bx_v \rangle = a^2 x_u^2 + 2abx_u x_v + b^2 x_v^2$$

$$(1.5)$$

Or

$$I = a^2 E + 2abF + b^2 G \qquad (1.6)$$

Where

$$E = x_u . x_u$$
$$F = x_u . x_v$$
$$G = x_v . x_v$$

$$(1.7)$$

In view of matrix we can express the first fundamental form as follows

$$I = \begin{pmatrix} a & b \end{pmatrix}^T \begin{pmatrix} E & F \\ F & G \end{pmatrix} \begin{pmatrix} a & b \end{pmatrix}$$

$$(1.8)$$

The matrix of x mapping is $\begin{pmatrix} E & F \\ F & G \end{pmatrix}$

$$(1.9).$$

1. 3.   The second fundamental form

In differential geometry, the Gauss map as in Fig 1.3 maps a surface in R^3 to the unit sphere S^2. Namely, given a surface U laying in R^3, the Gauss map is a continuous map $N : U \to S^2$ such that N(p) is a unit vector orthogonal to U at P, namely the normal vector to U at P.
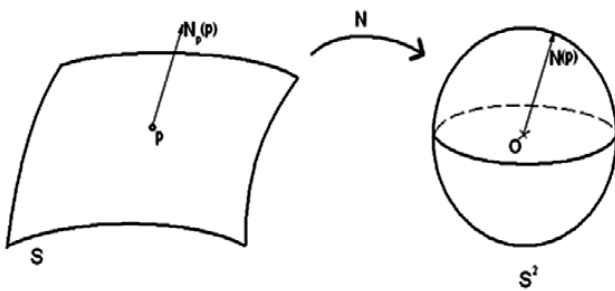
Fig. 1. 3 Gauss map

The composition of x map and N, Gauss map has the Second fundamental form.

Let me show you the quantity measure of the Second fundamental form [1-6] as follows

$$II = \langle d\omega, dN \rangle = \langle d^2\omega, \mathrm{N} \rangle \qquad (1.10)$$

Since $\mathsf{w} = ax_u + bx_v$ it is defined

$$d^u \mathsf{w} = ax_{uu} + bx_{vu}$$
$$d^v \mathsf{w} = ax_{uv} + bx_{vv}$$
$$d^2 \mathsf{w} = d^{uv} \mathsf{w} = (ax_{uu} + bx_{vu}).(ax_{uv} + bx_{vv}) = a^2 x_{uu} + 2abx_{uv} + b^2 x_{vv}$$

Then we obtain $\qquad (1.11)$

$$II = \langle d^2 \mathsf{w}, N \rangle = a^2 x_{uu}.N + 2abx_{uv}.N + b^2 x_{vv}.N$$

$$(1.12)$$

Where $N = \dfrac{x_u \times x_v}{\|x_u \times x_v\|}$ is unit Normal vector of the surface

U $\qquad e = x_{uu}.N$
If we set $\qquad g = x_{vv}.N$
$$f = x_{uv}.N = x_{vu}.N$$

then the second fundamental form can be written as

$$II = a^2 e + 2abf + b^2 g \qquad (1.13)$$

In view of matrix we can express the first fundamental form as follows

$$II = \begin{pmatrix} a & b \end{pmatrix}^T \begin{pmatrix} e & f \\ f & g \end{pmatrix} \begin{pmatrix} a & b \end{pmatrix}$$
$$(1.14)$$

The matrix of xoN mapping is

$$\begin{pmatrix} e & f \\ f & g \end{pmatrix}$$
$$(1.15).$$

1. 4.   Gauss curvature

The Gauss curvature, is considered as the extended of the line curvature in two dimension. Basically, the Gauss curvature is derived the first time by the very famous mathematician Carl Friedrich Gauss [1-6].

Given the surface parameterization and coordinate chart x, the first fundamental form is

$$I = a^2 E + 2abF + b^2 G \qquad (1.16)$$

Where

$$E = x_u.x_u$$
$$F = x_u.x_v$$
$$G = x_v.x_v \qquad (1.17)$$

The second fundamental form is

$$II = a^2 e + 2abf + b^2 g \qquad (1.18)$$

Where

$$e = x_{uu}.N$$
$$g = x_{vv}.N$$
$$f = x_{uv}.N = x_{vu}.N \qquad (1.19)$$

It is defined the Gauss curvature, $K(p)$, is ratio of the determinant of the second fundamental form to that of the first fundamental form [1–2].

$$K(p) = \frac{\det II}{\det I} = \frac{\begin{pmatrix} e & f \\ f & g \end{pmatrix}}{\begin{pmatrix} E & F \\ F & G \end{pmatrix}} \qquad (1.20).$$

$$K(p) = \frac{eg - f^2}{EG - F^2} \qquad (1.21)$$

Gauss theorem:

The Gauss curvature K is intrinsic, it means that it can be expressed completely by the elements E,F, and G the first fundamental form and surface parameterization x.
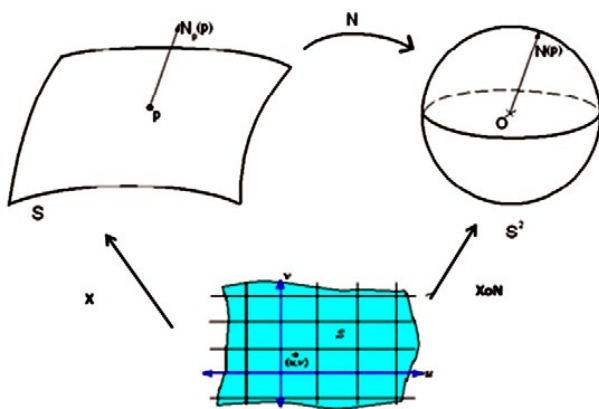
Fig. 1.4 Gauss curvature

1. 5.   Geodesic equation

Let us introduce about the vibrational problem which going back to the 18th century and is the main work of Karen Uhlenbeck around 1980 [7–9].

We have a functional

$$F(u) = \int \Phi(u, u') dx \qquad (1.22)$$

defined on functions u of one variable x.

The Euler-Lagrange equation associated to the functional is given by

$$\delta F = \int \delta u \tau(u) dx$$
$$\tau(u) = \frac{\partial \Phi}{\partial u} - \frac{d}{dx} \frac{\partial \Phi}{\partial u'} \qquad (1.23)$$

The Euler–Lagrange equation is.

Depending on the context, the functions would be required to satisfy suitable boundary conditions or, as in most of this article, might be defined on a compact manifold rather than a domain in Rⁿ, and u might not exactly be a function but a more complicated differential geometric object such as a map, metric, or connection.
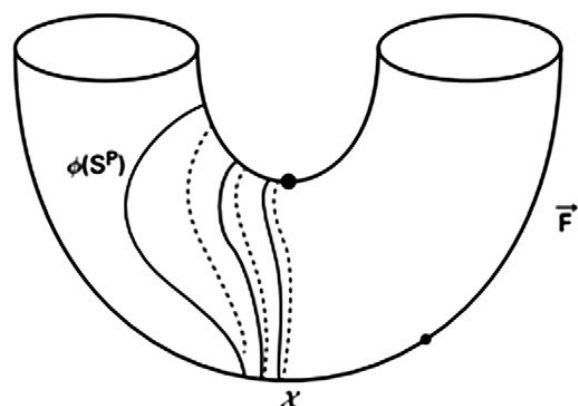
Fig.1.5 Critical point with a minimax sequence. The result is reproduced from [9]

One interprets $\tau(u)$, defined as in (1.23), as the derivative at u of the functional F on a suitable infinite dimensional space X and the solutions

of the Euler-Lagrange equation are critical points of F. If the functional F is bounded below one might hope to find a solution of the Euler-Lagrange equation which realizes the minimum of F on X. Fig 5 show finding a critical point with a minimax sequence.

The solutions to a variation problem in one dimension are geodesics in a Riemannian manifold.

Here we take N to be a compact, connected, Riemannian manifold and fix two points p, q in N. We take X to be the space of smooth paths $\gamma : [0,1] \to N$ with, $\gamma(0) = p, \gamma(1) = q$ and the energy functional

$$F(\gamma) = \int_0^1 |\nabla \gamma|^2 \quad (1.24)$$

Where the norm of the "vector velocity" $\nabla \gamma$ is computed using the Remannian metric on N.

The Euler-Langrange equation is the geodesic equation, in local co-ordinates [9-10],

$$\gamma_i'' - \sum_{j,k} \Gamma_{jk}^i \gamma_j' \gamma_k' = 0 \quad (1.25)$$

Where the "Christoffel symbols" Γ_{jk}^i are given by well-known formula in terms of metric tensors and its derivatives. In this case, the variational picture works as well as one could possibly wish. There is a geodesic from p to q minimizing the energy. More generally, one can use minimax arguments and (at least if p and q are taken in general position) the Moose theory [10] asserts that the homology of the path space X can be computed from a chain complex with generators corresponding to geodesics from p to q.

1. 6. Iso-metric mapping

Considering a manifold M which consists of CSDM (Cross-spectral density matrix) matrices and is equipped with inner product g_m on the tangent space $T_M(m)$. Given the inner product g_m on $T_M(m)$, each point m that varies smoothly from point to point in the sense that if X and Y are differentiable vector fields on M, then $m \to g_m(X|_m, Y|_m)$ is a smooth function [3,11].

Iso-metric mapping [3,11]

Let the mapping $f : E \to M$ where $\tilde{m} \in \tilde{E}, m \in M$ M is CSDM matrix manifold and $\tilde{E}$ is subspace of Euclidean space.

If the Riemannian metric on M is given by

$$g_m \langle a,b \rangle = \langle a,c \rangle \quad (1.26)$$

Where $a,b \in T_M(m)$ and c is matrix which is satisfied some rules in order to the necessary and sufficient that $a,b \in T_M(m)$ then $T_M(m)$ and $T_{\tilde{E}}(\tilde{m})$ are isometric.

Suppose that we have two points m_a and m_b on M. Parameterization of smooth curved path on M connecting m_a and m_b is a smooth function $\gamma : \theta \mapsto M$ in which $\theta \in R$ and θ is an open interval with their limits $\theta_a \leq \theta \leq \theta_b$.
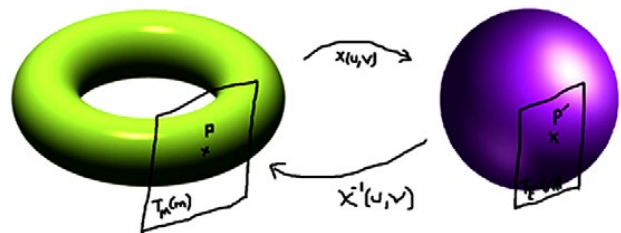
Fig. 1.6 An example of Iso-metric mapping

An example of iso-metric mapping is shown in Fig. 1.6. It is the mapping from the tangent space of a torus into the a tangent space of unit sphere. In general, the torus could be replaced by any kind of Riemannian manifold.

The length of the path between the two points is calculated as

$$l(m) = \int_{\theta_a}^{\theta_b} \sqrt{g_m(m',m')} d\theta \quad (1.27)$$

where $m' = \dfrac{dm}{d\theta}$, and $g_m(m',m')$ is an inner product in the tangent space, $T_M(m)$, at m on M.

The Riemannian distance between the two points is defined as the length of the geodesic, i.e.,

$$d_R(m_a, m_b) = \min_{m(\theta):[\theta_a,\theta_b] \mapsto M} \{l(m(\theta))\} \quad (1.28)$$

The length of a geodesic connecting m_a and m_b in M has the same length of geodesic connecting m_a and m_b in E as a result of the iso-metric mapping.

Therefore, we can derive the Riemannian distance by Euclidean distance as follows

$$d_R(m_a, m_b) = d_E(\tilde{m}_a, \tilde{m}_b)$$

(1.29)

Bibliography

1. M. Raussen, Elementary differential geometry: Curves and Surfaces, Department of Mathematical Sciences, Aalborg University, Denmark, 2008

2. T. Shifrin, Differential Geometry: A first course in curves and surfaces, Department of Mathematics, University of Georgia, USA, 2013

3. E. Kreyszig, Differential Geometry, Oxford University Press, 1959

4. Olivier Biquard, Introduction to differential geometry, Institute de Mathematiques de Jussieu, Universite Paris 06, France, 2008

5. P. Petersen, Classical Differential Geometry, Lecture note, UCLA

6. J. W. Robbin and D. A. Salamon, Introduction to Differential Geometry, Department of Mathematics, University Wisconsin Madison, USA

7. I. M. Gelfand and S. V. Fomin, Calculus of variations, Prentice Hall Inc, 1963

8. R. Weinstock, Calculus of Variations with applications to physics and engineering, Dover Publications Inc, New York, 1974

9. S. Donaldson, Karen Uhlenbeck and the calculus of variations, Notices of the Mathematical Society, March 2019, pp.303-313

10. J. Baez and J. P. Muniain, Gauge field, knots and gravity, World Scientific Publishing Co. Pte. Ltd, 1994

11. T. C. Quyen, Matched field processing for source localization based on an approach of Riemannian geometry, AKSUTIKA, Vol.33, pp.71-71, 2019.

CHAPTER 2.

MATCHED FIELD PROCESSING

The aim of this chapter is introduce the Matched field processing (MFP). There are two approaches. In the first one, environmental parameters are bringing into the signal processing model so that MFP could be adaptive to the variation of the environment. In the second one, MFP is considered as a robust signal processing instead of optimum signal processing as usual in statistical signal processing.

2.1 The first approach of Matched field processing

Let us introduce the subject of Matched field processing by considering the MFP as the signal processing method [1–8] which is embedded the environmental parameters as in Fig.1 as follows
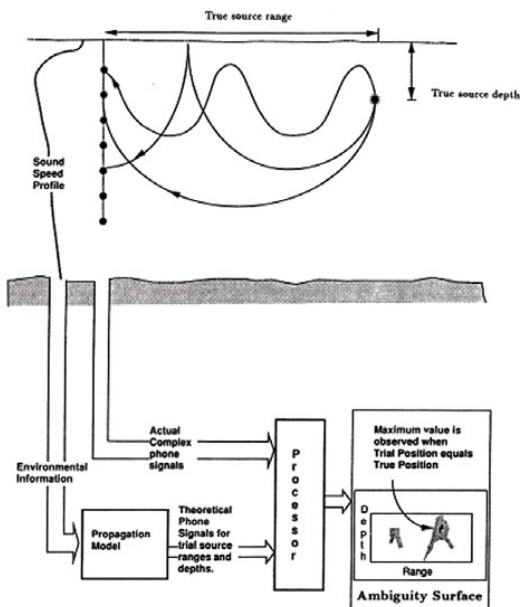
Fig. 2.1 Basic components of MFP. The result is reproduced from [2]

From the Fig. 2.1 it is clear that the processor of MFP in general using two kinds of signal. The first signal is environmental information and the second signal is measured signal coming from a vertical, horizontal or cylindrical hydrophone array.

It is important to emphasis about the environmental information, we could collect as much as possible but at least the sound speed profile (SSP) must be achieved.

If we consider the deep ocean as a single duct with rms sea surface roughness $\sigma = 2\,m$, and a totally absorbing bottom the SSP is depicted as follows
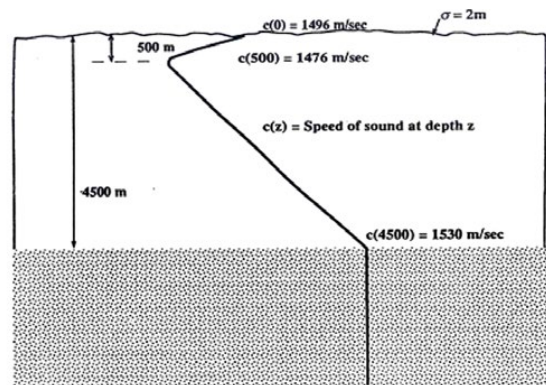
Fig. 2.2. Environmental parameters representing a single duct deep ocean sound–speed profile, rms sea surface roughness, $\sigma = 2\,m$, and a totally absorbing bottom. The result is reproduced from [2].

In reality, the reflecting bottom is made of sand or mud or a composite of sand and mud. The deep sediment layer is over 500 m and has elastic property. Typical relative densities of those layers are illustrated as in Fig. 2.3 as follows
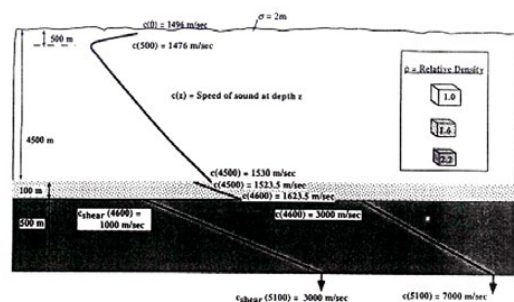
Fig. 2.3. Environmental parameters illustrating reflecting bottom consisting of a 100 m deep sediment layer over a 500 m deep elastic layer over an elastic half–space. s The result is reproduced from [2].

The fact that, the ocean environment could vary from place to place. In some case, we have to deal with the double duct (double oceanic waveguides) as in Fig. 2.4 as follows
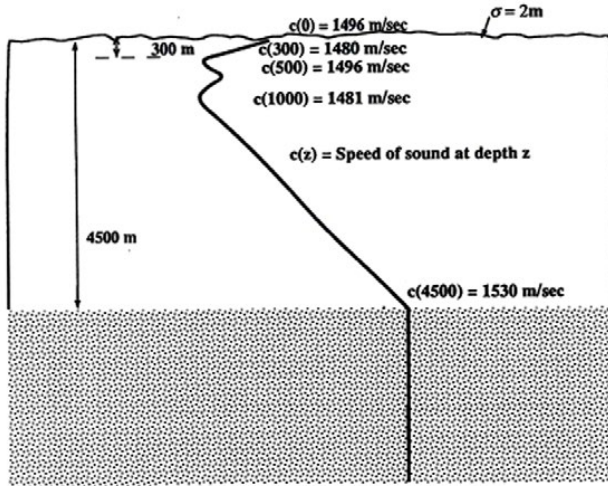
Fig. 2.4. Environmental parameters for double duct deep ocean sound–speed profile. Bottom is totally absorbing. The result is reproduced from [2].

The main idea here is MFP is not only processing the signal from the hydrophone arrays but also the signal from the propagation models.

2.2 Propagation models

2. 2. 1. The Normal Mode

Staring from Helmholtz equation in two dimensions with sound speed c and density ρ depending only on depth z [9-14]

$$\frac{1}{r}\frac{\partial}{\partial r}(r\frac{\partial \psi}{\partial r})+\rho(z)\frac{\partial}{\partial z}(\frac{1}{\rho(z)}\frac{\partial \psi}{\partial z})+\frac{\omega^2}{c(z)^2}\psi=-\frac{\delta(r)\delta(z-z_s)}{2\pi r}$$

(2.1)

where z_s is source depth, z is depth and r is distance.

Using separation of variables $\psi(\mathrm{r},z)=\Phi(\mathrm{r}).\mathrm{V}(z)$ we obtain the modal equation

$$\rho(z)\frac{d}{dz}[\frac{1}{\rho(z)}\frac{dV_m(z)}{dz}]+[\frac{\omega^2}{c(z)^2}-k_{rm}^2]V_m(z)=0$$

(2.2)

with the boundary conditions such as

$$V(0)=0,\frac{dV}{dz}\Big|_{z=D}=0$$

(2.3).

The former condition implies a pressure release surface and the latter condition is from a perfect rigid bottom. The modal equation that is the center of the NM, has an infinite number of modes. Each mode represents by a mode amplitude $V_m(z)$ and a horizontal propagation constant k_{rm}. $V_m(z)$ and k_{rm} are also called *eigenfunction* and *eigenvalue* respectively

Noting that the modes are orthonormal, i.e.,

$$\int_0^D \frac{V_m(z)V_n(z)}{\rho(z)}dz=0, \quad \mathrm{m}\neq \mathrm{n}$$

$$\int_0^D \frac{V_m(z)^2}{\rho(z)}dz=1$$

(2.4)

Since the modes forms a complete set, the pressure can represents as a sum of the normal modes

$$\psi(r,z)=\sum_{m=1}^{\infty}\Phi_m(r)V_m(z)$$

(2.5)

After some manipulations, we obtain

$$\psi(r,z)=\frac{i}{4\rho(z_s)}V_m(z_s)H_0^1(k_{rm}r)$$

(2.6)

where H_0^1 is the Hankel function of the first kind.

Substitute (6) back to (5) we have

$$\psi(r,z)=\frac{i}{4\rho(z_s)}\sum_{m=1}^{\infty}V_m(z_s)V_m(z)H_0^1(k_{rm}r)$$

(2.7)

Finally, using the asymptotic approximation of the Hankel function, the pressure can be written as

$$\psi(r,z)\approx\frac{i}{\rho(z_s)\sqrt{8\pi r}}e^{-i\pi/4}\sum_{m=1}^{\infty}V_m(z_s)V_m(z)\frac{e^{ik_{rm}r}}{\sqrt{k_{rm}}}$$

(2.8)

2. 2. 2. The Parabolic Equation

Starting from the Helmholtz equation in the most general form [12]

$$\nabla^2 \psi + k_0^2(n^2-1)\psi = 0 \qquad (2.9)$$

where n is the refraction index of the medium and k_0 is the wavenumber at the acoustic source.

In cylindrical coordinate, (1) becomes

$$\psi_{rr} + \frac{1}{r}\psi_r + \psi_{zz} + k_0^2(n^2-1)\psi = 0$$

$$(2.10)$$

in which the subscripts denote the order of derivative.

From the assumption of Tappert [13-14], ψ is defined as

$$\psi(r,z) = \Phi(r,z)V(r) \qquad (2.11)$$

where z denotes depth and r denotes distance.

Thus (2.10) becomes the system of equations as follows

$$\Phi_{rr} + \left(\frac{1}{r} + \frac{2}{V}V_r\right)\Phi_r + \Phi_{zz} + k_0^2(n^2-1)\Phi = 0$$

$$(2.12)$$

and

$$V_{rr} + \frac{1}{r}V_r + k_0^2 V = 0 \qquad (2.13)$$

The root of (13) is a Hankel function with its approximation as

$$V_{r0} = H_0^1(k_0 r) = \sqrt{\frac{2}{\pi k_0 r}} e^{i(k_0 r - \frac{\pi}{4})}$$

$$(2.14)$$

After some manipulations, (2.12) becomes

$$2ik_0\Phi_r - \Phi_{zz} + k_0^2(n^2-1)\Phi = 0 \qquad (2.15),$$

i.e. a parabolic equation.

Taking the Fourier transform both side of (2.15) in z domain obtained

$$2ik_0\Phi_r - k_z^2\Phi + k_0^2(n^2-1)\Phi = 0 \qquad (2.16)$$

Rewrite (2.16) in simpler form as

$$\Phi_r + \frac{k_0^2(n^2-1) - k_z^2}{2ik_0}\Phi = 0 \qquad (2.17)$$

Thus, from [9] we have

$$\Phi(r,\mathrm{k}_z) = \Phi(r_0,\mathrm{k}_z)e^{\frac{-k_0^2(n^2-1)-k_z^2}{2ik_0}(r-r_0)} \qquad (2.18)$$

where $\Phi(r_0,\mathrm{k}_z)$ is the initial value of the source.

Taking the Inverse Fourier transform both side of (2.18) obtained

$$\Phi(r,z) = e^{i\frac{k_0}{2}(n^2-1)\Delta r}\int_{-\infty}^{\infty}\Phi(r_0,\mathrm{k}_z)e^{\frac{-i\Delta r k_z^2}{2ik_0}}e^{ik_z z}dk_z$$

$$(2.19)$$

where $\Delta r = r - r_0$.

Finally, we arrived

$$\Phi(r,z) = e^{i\frac{k_0}{2}(n^2-1)\Delta r}\Im^{-1}\left\{e^{\frac{-i\Delta r k_z^2}{2ik_0}}\Im\{\Phi(r_0,z)\}\right\}$$

$$(2.20).$$

This form is called Split–Step Fourier transform.

2. 2. 3. Simulation Results

In this simulation, Tonkin gulf is used as Pekeris waveguide model with its sound velocity which is measured from [15]. Thuc was carried out many sound speed measurements which were reported in his monograph. On the basis of Thuc's results, the medium parameters of Tolkin gulf are given in the Table 2.1 as follows

Table 2.1. The medium parameters

Paremeter	Value
Ocean depth	100 m
Sound speed in winter	c(z)=1500+0.3z (m/s)
Bottom	Sand, ρ_1=2000 kg/m³ c_1=1700 m/s
Point source	f=250 Hz, h= 99 m
Noise	Gaussian, SNR=3dB

In Table 2.1, c denotes sound velocity whereas ρ indicates medium density.

The transmission loss factors (TLs) of NM and PE are shown [16] in Fig. 2.5 and Fig. 2.6.
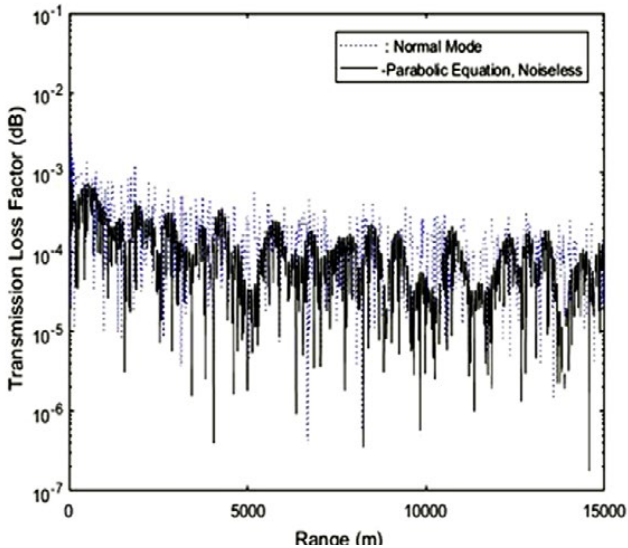
Fig.2.5. Transmission loss factors of NM and PE with range up to 15 km, noiseless case.
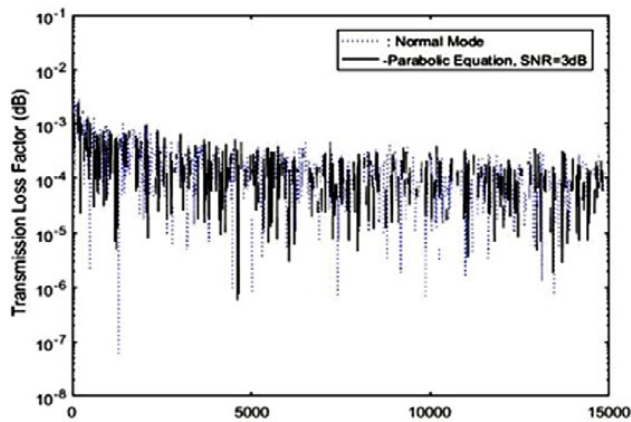
Fig. 2.6 Transmission loss factors of NM and PE with range up to 15 km, SNR=3dB.

From Fig. 2.5 and Fig. 2.6 we can see clearly that the TLs of both NM and PE with range up to 15 km far from the acoustic source. In the conditions of this simulation, this TLs are stable after hundreds of simulations. Further, there is the agreement of TLs between NM and PE.

In the first case (noiseless case), from Fig. 2.5, the TL of PE seems reducing to distance more slightly than the TL of NM. It is basically, could be thought of the nature of range dependence of PE approach.

In the second case (when SNR of 3 dB), from Fig. 2.6, the agreement of TLs of both methods is more consistent since the signal level in this case is higher than the noise level and it is compensated for a long range transmission.

The computation of PE is slightly more than NM (it is not shown here).

2.3 The second approach of Matched field processing

Let us introduce the second approach of Matched field processing which is called robust signal processing [17-19]. Fig. 2.7 is an explanation of the concept of robust signal processing.
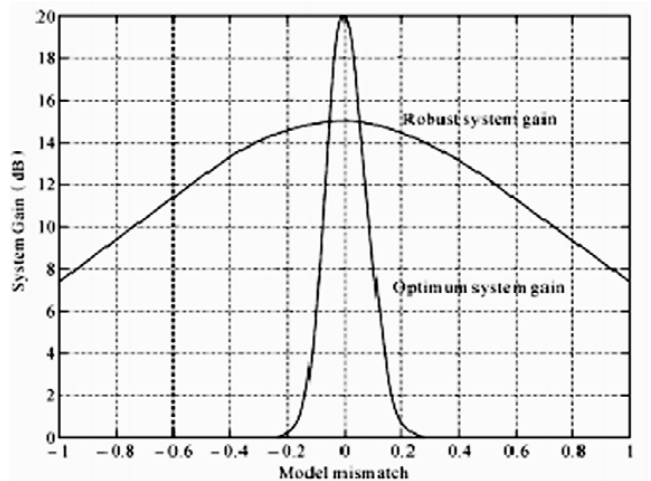
Fig. 2.7. Concept of robust detection. The result is reproduced from [19]

In an ideal situation the system gain from robust signal processing is less than that of optimum signal processing. But robust signal processing is not sensitive to model mismatch, i.e., in the case of model mismatch, the system gain of robust signal processing is larger than that of optimum signal processing, which is what we can expect most frequently.

The following explanation is come from [19]

Suppose H is a possible sonar design space, the element of this space is the possible signal processing method. Q is a set of consisting of various models. Define a metric function $M(h,q), h \in H, q \in Q$, which is used to measure the system performance using model q and signal processing method h.

The traditional sonar design is for fixed $q_0 \in Q$. Find $h_0 \in H$ such that

$$M(h_0, q_0) = \max_{h \in H} M(h, q_0) \qquad (2.21)$$

That means $h_0 \in H$ is the optimum signal processing method for model $q_0 \in Q$.

If the real ocean environment model q_0 is varying, it can be changed in a subset P of Q, i.e., the element of model $p \subset P \in Q$. In this situation, how to choose the signal processing method? A reasonable strategy is to use the maximum-minimum method in game theory. That means for any $h \in H$ find q, which minimizes M(h,q). An then find h, which maximizes the value of $\min_{q \in P} M(h, q)$, i.e.,

$$\max_{h \in H} \min_{q \in P} M(h, q) \qquad (2.22)$$

The robust signal processing method, h_R, is the signal processing method which satisfies the following equation

$$\min_{q \in P} M(h_R, q) = \max_{h \in H} \min_{q \in P} M(h, q) \qquad (2.23)$$

2.4 Properties of Matched Field Processing

The properties of matched field processing are described detail in [2]. Fig. 2.8 illustrate those properties.
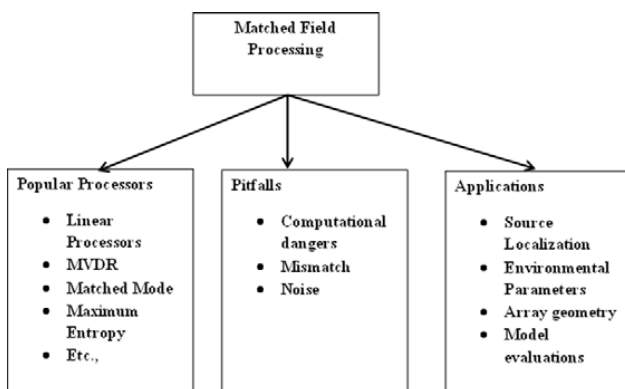
Fig. 2.8. Properties of Matched Field Processing

Among them [20-25], the popular processors are linear, MVDR, matched mode, maximum entropy, etc., The linear processor is considered as the base for the comparison to other processors.

When the expert involves into the matched field processing, one have to cope with the computational danger such as matrix inversion or sampling of the cross spectral matrix coming from measured data. The model mismatched is always the case happening in reality and it affected the system performance in vary large scale.

The noise in reality is considered as color and broadband noise but is not uniform, homogeneous and isotropic as normal assumption.

In term of the application, MFP is the most effective way to underwater source localization. The other application are determine the environmental parameters such as sound speed profile and water, sediment densities, etc.,

Since it is inverse problem so we can exploit the method as a tool for model evaluations which including ray, normal mode and parabolic approximation model.

Bibliography

1. A, Tolstoy, Application of matched field processing to inverse problems in underwater acoustics. IOP science, 16(6),p.1655-1666, 2000, DOI: https:// doi.org/10.1088/0266-5611/16/6/304

2. A. Tolstoy, Matched Field Processing for Underwater Acoustics, World Scientific, 1993

3. A. Tolstoy, W. AU, The matched field processing of binaural dolphin-like signals for the detection and identification of buried targets, Journal. Com. Acoustics, Vol.11, No.4, pp. 521-534, 2003.

4. A. Tolstoy, Waveguide monitoring (such as sewer pipes or ocean zones) via matched field processing, J.Acoust.Soc.Am, 128(1), 2010

5. A. Tolstoy, Matched field processing (MFP)-Based inversion method (SUB-RIGS) for Range-Dependent Scenarios, IEEE Journal. Oceanic. Engineering, Vol.29, No.1, pp. 59-77, 2004

6. A. Tolstoy, Sensitivity of matched field processing to sound speed profile mismatch for vertical arrays in a deep water Pacific environment, J. Acoust. Soc. Am 85(6), pp.2394-2404, 1989

7. A. B. Baggeroer, W. A. Kuperman. P. N. Mikhalevskey, An overview of matched field methods in ocean acoustics. IEEE J. Ocean Engineering, 18 (4), p. 401-424, 1993

8. A. B. Baggerorer, W. A. Kuperman, H. Schmidt, Matched field processing: Source localization in correlated noise as an optimum parameter estimation problem. J. Acoustic. Soc. Am. 83(2), p. 571-587, 1988

9. W. A. Strauss, Partial differential equations an introduction, John Wiley and Sons, Inc, 1992

10. R. J. Urick, Principle of underwater sound, McGraw-Hill Book Company, 1983

11. X. Lurton, An introduction to underwater acoustics: principles and applications, Praxis Publishing Ltd, UK, 2002

12. J. B. Kuperman et al, Computational Ocean Acoustics, Springer, 2011

13. F. D. Tappert, "The parabolic approximation method", Wave propagation in underwater acoustics, pp.224-287, Springer, New York, 1977.

14. D. Lee, "The state of the art parabolic equation approximation as applied to underwater acoustic propagation with discussion on intensive computations", J. Acoutic. Soc. Am, 76, 1984.

15. Pham Van Thuc, Ocean Sound and Sound Field in South East Asia Sea, National and Science Technology Express, 2011.

16. T. C. Quyen, Normal mode vs Parabolic equation and their application in Tonkin gulf, Journal of Science and Technology, Vol.53, pp.3-9, 2019, ISSN: 1859-3585

17. S. Stergiopoulos, Advanced signal processing handbook, CRC Press, 2018

18. M. A. Ainslie, Principles of SONAR performance modeling, Springer, 2010

19. Q. Li, Digital Sonar design in underwater acoustics: principles and applications, Springer, London, New York, 2012

20. R. Klemm, Interrelations between matched field processing and airbone MTI radar, IEEE Journal. Oceanic. Engineering, Vol.18, No.3, pp. 168-180, 1993

21. R. Klemm, Range and depth estimation by line arrays in shallow water, Signal Processing 3, 333-344, 1981

22. H. P. Bucker, Use of calculated sound fields and matched field detection to locate sound sources in shallow water, J. Acoust. Soc. Am, 59(2), pp.368-373, 1976

23. M. Porter and A. Tolstoy, The matched field processing benchmark problems, Journal. Com. Acoust, 2(3), 161-185, 1994

24. J. M. Ozard, Matched field processing in shallow water for range, depth, and bearing determination: Results of experiment and simulation, J. Acoust. Soc. Am. 86(2), 744-753, 1989

25. K. L. Gemba, W. S. Hodgkiss, and P. Gerstoft, Adaptive and compressive matched field processing, J. Acoust. Soc. Am. 141, 92-103, 2017

CHAPTER 3. RIEMANNIAN MATCHED FIELD PROCESSING

Let us introduce the class of Matched Field Processing, namely Riemannian Matched Field Processing (RMFP), by considering the Riemannian distance instead of Euclidean distance. It is the purpose of this chapter and of this monograph. Therefore, not only the nature of curvature of sound wave in Chapter 1 but also the nature of Matched Field Processing in Chapter 2 are exploited in RMFP. Two approaches of RMFP construction, i.e., iso-metric mappings and direct Riemannian distance calculation are introduced.

3.1 RMFP based on iso-metric mapping

The fact that Cross Spectral Density Matrices (CSDMs) which are not randomly but Hermite and positive definite, form a manifold that each CSDM is a point on it.

Considering a manifold M which consists of CSDM (Cross-spectral density matrix) matrices and is equipped with inner product g_m on the tangent space $T_M(m)$. Given the inner product g_m on $T_M(m)$, each point m that varies smoothly from point to point in the sense that if X and Y are differentiable vector fields on M, then $m \rightarrow g_m(X|_m, Y|_m)$ is a smooth function.

Suppose that we have two points m_a and m_b on M. Parameterization of smooth curved path [1–3] on M connecting m_a and m_b is a smooth function $\gamma : \theta \mapsto M$ in which $\theta \in R$ and θ is an open interval with their limits $\theta_a \le \theta \le \theta_b$. In general, the length of the path between the two points is calculated as

$$l(m) = \int_{\theta_a}^{\theta_b} \sqrt{g_m(m', m')} d\theta \qquad (3.1)$$

where $m' = \dfrac{dm}{d\theta}$, and $g_m(m', m')$ is an inner product in the tangent space, $T_M(m)$, at m on

M. The Riemannian distance between the two points (Fig. 3.1) is defined as the length of the geode sic, i.e.,

$$d_R(m_a, m_b) = \min_{m(\theta):[\theta_a, \theta_b] \mapsto M} \{l(m(\theta)\} \qquad (3.2)$$
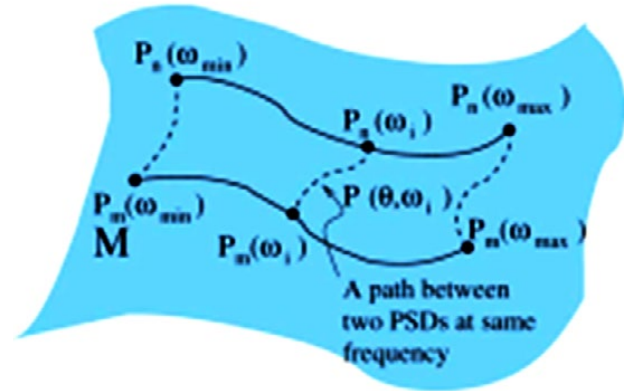
Fig. 3.1 Riemannian distance between CSDM matrices of two signals. The result is reproduced from [1]

Theorem 1: The condition of existing the iso-metric mapping

Let the mapping $f : E \rightarrow M$ where $\tilde{m} \in \tilde{E}, m \in M$, M is CSDM matrix manifold and $\tilde{E}$ is subspace of Euclidean space.

If the Riemannian metric on M is given by

$$g_m \langle a, b \rangle = \langle a, c \rangle \qquad (3.3)$$

Where $a, b \in T_M(m)$ and c is matrix which is satisfied some rules in order to the necessary and sufficient that $\langle a, b \rangle = \langle a, c \rangle = g_m$ then $T_M(m)$ and $T_{\tilde{E}}(\tilde{m})$ are isometric.
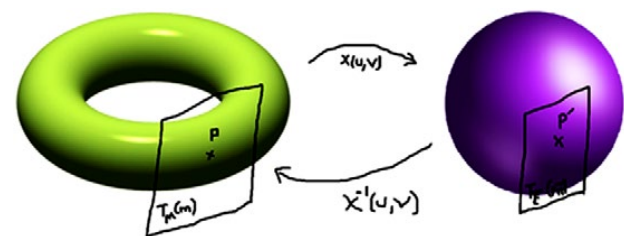
Fig. 3.2 An example of iso-metric mapping

An example of iso-metric mapping is shown in Fig. 3.2. It is the mapping from the tangent space of a torus into the a tangent space of unit sphere. In general, the torus could be replaced by any kind of Riemannian manifold.

The length of a geodesic connecting m_a and m_b in M has the same length of geodesic connecting m_a and m_b in $\tilde{E}$ as a result of the iso-metric mapping.

Therefore, we can derive the Riemannian distance by Euclidean distance as follows

$$d_R(m_a, m_b) = d_E(\tilde{m}_a, \tilde{m}_b) \qquad (3.4)$$

The RMFP classifications [4-6] based on different iso-metric mappings as in Fig. 3.3 as follows
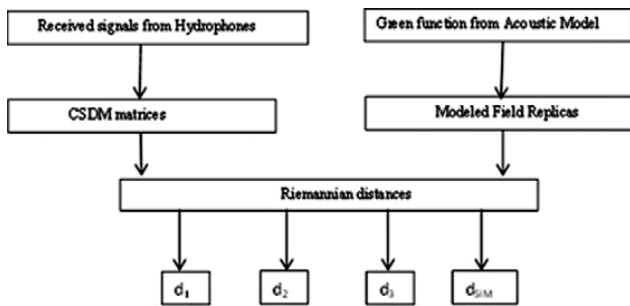
Fig. 3.3 Classification of RMFP based on different iso-metric mappings

There are 4 kinds of iso-metric mappings corresponding to 4 kinds of Riemannian Matched Field Processing as follows [2,4]

$$(\hat{r}_s, \hat{z}_s)_{d_1} = \underset{\hat{p}}{\textbf{argmin}} \sqrt{tr(\textbf{R}_{p_s}) + tr(\textbf{R}_{\hat{p}}) - 2tr(\textbf{R}_{p_s} \textbf{R}_{\hat{p}})}$$

$$(3.5)$$

$$(\hat{r}_s, \hat{z}_s)_{d_2} = \underset{\hat{p}}{\textbf{argmin}} \sqrt{tr(\textbf{R}_{p_s}) + tr(\textbf{R}_{\hat{p}}) - 2tr(\textbf{R}_{p_s}^{1/2} \textbf{R}_{\hat{p}}^{1/2})}$$

$$(3.6)$$

$$(\hat{r}_s, \hat{z}_s)_{d_3} = \underset{\hat{p}}{\textbf{argmin}} \sqrt{\sum_k ln^2 \lambda_k}$$

$$(3.7)$$

where λ_k is eigenvalues of $\textbf{R}_{p_s}^{-1} \textbf{R}_{\hat{p}}$

$$(\hat{r}_s, \hat{z}_s)_{d_{SIM}} = \underset{\hat{p}}{\textbf{argmin}} \sqrt{tr[(sin\textbf{R}_{p_s})^2] + tr[(sin\textbf{R}_{\hat{p}})^2] - 2tr[sin(\textbf{R}_{p_s})sin(\textbf{R}_{\hat{p}})]}$$

$$(3.8)$$

Where $\hat{r}_s$ is the estimated range of the source, $\hat{z}_s$ is the estimated depth of the source, $\hat{p} = (\hat{r}_s, \hat{z}_s)$ is true source coordinate, $\textbf{R}_{p_s}$ is CSDM of collected data and $\textbf{R}_p$ is CSDM of modeled field replicas.

3. 2.   3.2 RMFP based on direct Riemannian distance calculation

The fact that stochastic Matched Field Processing (SMTP) are derived on the basis of Riemannian distance (RDs) which were calculated using isometric mappings (IMs) [2,4].

If an IM does not exist, we must solve geodesic equations directly to find the geodesic distance.

The classification of RMFP based on directed Riemannian distance [5-6] is depicted in Fig.3.4 as follows
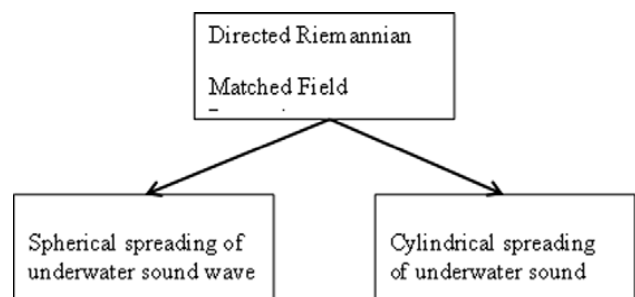
Fig. 3.4 Classification of RMFP based on directed Riemannian distances

There are two kinds of Direted RMFP i.e., on the basis of spherical spreading and of cylindrical spreading of underwater sound wave.

After solving the geodesic equations directly with assumption of spherical and cylindrical spreading, we found that the geodesic distance in the fashion of great circle (Fig. 3.5) for spherical spreading and in the fashion of helix (Fig. 3.6) for cylindrical spreading.

For detail of geodesic distance calculation, we referred the reader to the references [5-6].

Spherical Spreading [5]

First step:

The Riemannian matched field processor based on Riemannian geometry is received by obtaining the space coordinates of data replicas which are scanning over all modeled

field replicas position $\overset{\wedge}{\mathbf{p}} = (\overset{\wedge}{\mathbf{r}}_s, \overset{\wedge}{\mathbf{z}}_s)$ with a subject constraint of minimization of Riemannian distance as follows

$$(\hat{r}, \hat{z}) = \arg\min_{\overset{\wedge}{\mathbf{p}}} \sqrt{tr(\mathbf{R}_{\mathbf{p}_s}) + tr(\mathbf{R}_{\overset{\wedge}{\mathbf{p}}}) - 2\,tr(\mathbf{R}_{\mathbf{p}_s}\mathbf{R}_{\overset{\wedge}{\mathbf{p}}})}$$

(3.9)

Second step:

Now, on the basis of the outcome of directed Riemannian distance, we found that the geodesic distance of Spherical spreading is preferred to Great circle distance. This mean that

$$d_{\min} = \min(d_1, d_{Great\ Circle})$$

$$d_1 = \sqrt{tr(\mathbf{R}_{\mathbf{p}_s}) + tr(\mathbf{R}_{\overset{\wedge}{\mathbf{p}_s}}) - 2tr(\mathbf{R}_{\mathbf{p}_s}\mathbf{R}_{\overset{\wedge}{\mathbf{p}_s}})}$$

$$d_{Great\ Circle} = R\sqrt{(f(\theta) - f(\hat{\theta}))^2 + (\cos\theta - \cos\hat{\theta})^2}$$

$$f(\theta) = \sin\theta.\sin[\cos^{-1}(\cot g\theta)]$$

$$(\hat{r}_s, \hat{z}_s) = \arg\min_{\overset{\wedge}{\mathbf{p}}}(d_1, d_{Great\ Circle})$$

(3.10)

where
$R = radius\ of\ sphere$

$\theta = parameterization\ of\ modeled\ data$

$\overset{\wedge}{\theta} = parameterization\ of\ measurement\ data$
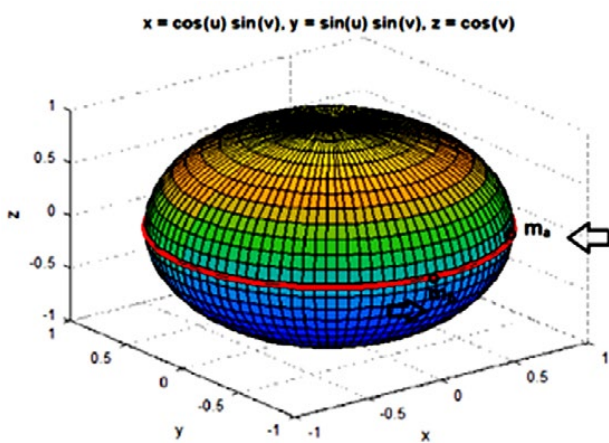
Fig. 3.5 The great circle (red line) between two fix points (m_a, m_b) on the surface of the 3D sphere.

Cylindrical Spreading [6]

First step:

The Riemannian matched field processor based on Riemannian geometry is received by obtaining the space coordinates of data replicas which are scanning over all modeled field replicas position $\overset{\wedge}{\mathbf{p}} = (\hat{r}, \hat{z})$ with a subject constraint of minimization of Riemannian distance as follows

$$(\hat{r}, \hat{z}) = \arg\min_{\overset{\wedge}{\mathbf{p}}} \sqrt{tr(\mathbf{R}_{\mathbf{p}_s}) + tr(\mathbf{R}_{\overset{\wedge}{\mathbf{p}}}) - 2\,tr(\mathbf{R}_{\mathbf{p}_s}\mathbf{R}_{\overset{\wedge}{\mathbf{p}}})}$$

(3.9)

Second step:

Now, on the basis of the outcome of directed Riemannian distance, we found that the geodesic distance of Cylindrical spreading is preferred to Helix distance. This mean that

$$d_{\min} = \min(d_1, d_{Helix})$$

$$d_1 = \sqrt{tr(\mathbf{R}_{\mathbf{p}_s}) + tr(\mathbf{R}_{\overset{\wedge}{\mathbf{p}_s}}) - 2tr(\mathbf{R}_{\mathbf{p}_s}\mathbf{R}_{\overset{\wedge}{\mathbf{p}_s}})}$$

$$d_{Helix} = \sqrt{(D\cos(t) - D\cos(\hat{t}))^2 + (ht - h\hat{t})^2}$$

$$(\hat{r}_s, \hat{z}_s) = \arg\min_{\overset{\wedge}{\mathbf{p}}}(d_1, d_{Helix})$$

(3.11)

where
$D = outer\ radius\ of\ Helix$

$h = pitch\ length$

$t = parameterization\ of\ modeled\ data$

$\hat{t} = parameterization\ of\ measurement\ data$
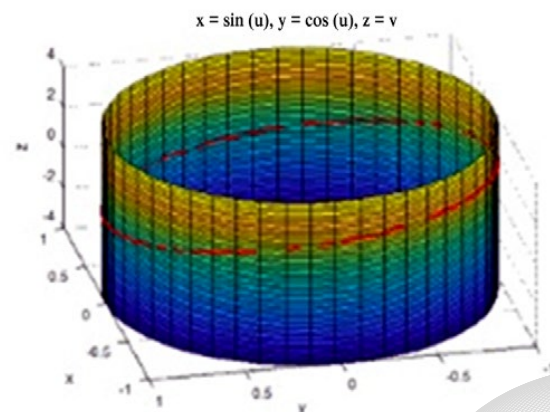
Fig.3.6 The helix (red line) on the surface of the 3D cylinder.

Bibliography

1. Y. Li, K. M. Wong, Riemannian distances for signal classification by power spectral density. IEEE. J. Sec. Top. Sig. Processing. **7**(4), p. 655-669, 2013

2. S. Finette and P. C. Mignerey, Stochastic matched field localization of an acoustic source based on principles of Riemannian geometry, J. Acoustic. Soc. Am 143 (6), p. 3628-3638, 2018

3. R. Cao et al, Passive broad band source localization based on a Riemannian distance with a short vertical array in the deep ocean, J. Acoustic. Soc. Am 145 (6), p. 567-573, June 2019.

4. T. C. Quyen, Matched field processing for source localization based on an approach of Riemannian geometry, AKSUTIKA, Vol.33, pp.71-71, 2019.

5. T. C. Quyen, Stochastic matched field processing using directed Riemannian distance, AKUSTIKA, Vol. 40, pp.2-6, 2021

6. T. C. Quyen, Underwater source localization using cylindrical hydrophone array and Riemannian matched field processing, AKUSTIKA, Vol. 42, pp. 6-12, 2022

CHAPTER 4. PERFORMANCE OF RIEMANNIAN MATCHED FIELD PROCESSING

Fig. 4.1 SSP of SACLANTC 1993 North Elba

In Chapter 2 the Matched Field Processing was treated as a robust signal processing. In Chapter 3 the Riemannian Matched Field Processing was considered in view of Riemannian Geometry. In this Chapter the Riemannian Matched Field Processing are continued but are extended to its performance. Following a section of input acoustic data, the performance of conventional Matched Field Processing is introduced. This is followed by a discussion of the performance of Riemannian Matched Field Processing using vertical hydrophone array as well as circular hydrophone array and cylindrical hydrophone array.

4. 1.   Input Acoustic Data

Passive array data SONAR from SACLANTC 1993 North Elba experiment available in Internet was used for processing [1].The vertical underwater acoustic array data was collected in shallow-water off the Italia west coast by the NATO SACLANTC Center in La Spezia, Italy. The original SACLANTC time series has been converted to a series of MATLAB .mat files each of which contains a matrix "dat" that is 48 sensors by 64K data points long. Each file represents about 1 minute of data. The vertical array consists of 48 hydrophones with spacing 2 m between elements at total aperture length 94 m (18.7 m to 112.7 m in depth). The source emitted PRN signal with center frequency of 170 Hz.

The Sound Speed Profile (SSP) from [1] is described in Fig. 4.1 as follows.

4. 2.   Performance of Conventional Matched Field Processing

Fig. 4.2 is obtained from conventional MFP in which only one modeled field and one replica of SONAR array data were used. It should be noted that the data is from SACLANTC and SNR level is -3 dB and the number of snapshot is greater than 20 samples It can be seen that the true source can be detected at depth of 60 m and range of 6000 m.
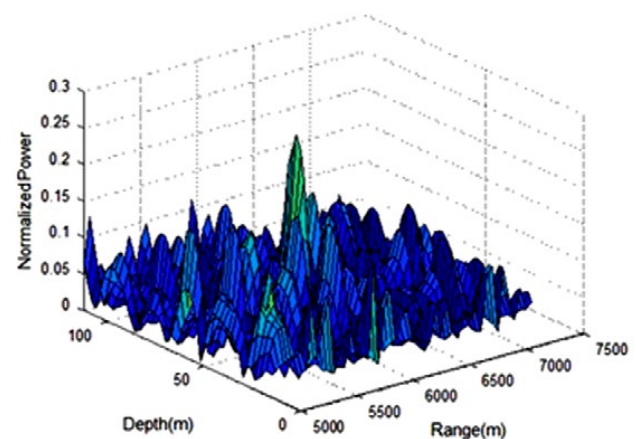
Fig. 4.2 a): Ambiguity surface of conventional matched field processing (one modeled field and one data replica, SNR=-3dB, No of snapshot>20 samples in 3 dimensions. The result is reproduced from [6].

Fig. 4.2 b): Ambiguity surface of conventional matched field processing (one modeled field and one data replica, SNR=-3dB, No of snapshot>20 samples in 2 dimensions. The result is reproduced from [6].
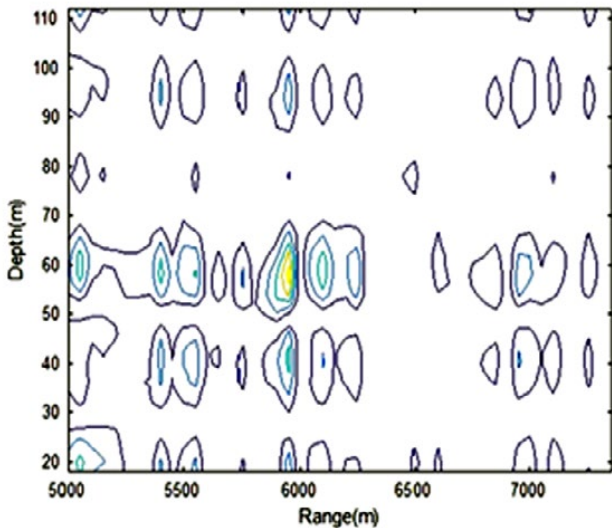
4. 3. Performance of Riemannian Matched Field Processing

4. 3. 1. Vertical Hydrophone Array (VHA)

The simplest possible example of a hydrophone array is vertical hydrophone array. The geometry of a vertical hydrophone array with 8 iso-tropic elements and its directivity are depicted as in Fig 4.3 as follows
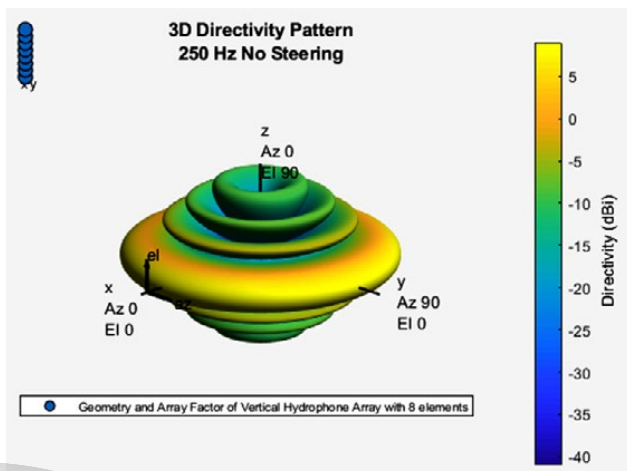
Fig. 4.3 The geometry of a vertical hydrophone array with 8 iso-tropic elements and its array factors

Each simulation uses 10 replicas of SONAR array data which provided by SACLANC and SNR level of 10 dB and the number of snapshot is greater than 30 samples. Twenty modeled field replicas are obtained from variable sound speeds that changed to depth according to SSP as depicted in Fig. 4.1 (In reality modeled field replicas could be caused from other factor such as internal-wave, bottom parameter mismatch and others).

From Fig. 4.4 it can be seen that the true source can be detected at depth of 60 m and range of 6000 m if 20 modeled field replicas and 10 data replicas were used for the proposed Riemannian matched field processor. In Fig. 4.5 the performance of the proposed Riemannian matched field processor used only 6 modeled field replicas shows that beside the true source location there are a number of spurious peak locations which are corresponding to ocean variability or mismatch conditions. Since the true source location is higher than other spurious peak locations, one can find it. However, we could not detect the source in the case in Fig. 4.6 when only 3 modeled field replicas were used and all peak location are almost equally. It is always the case of MFP when the number of modeled field replicas could not provide enough fluctuation of ocean environment.
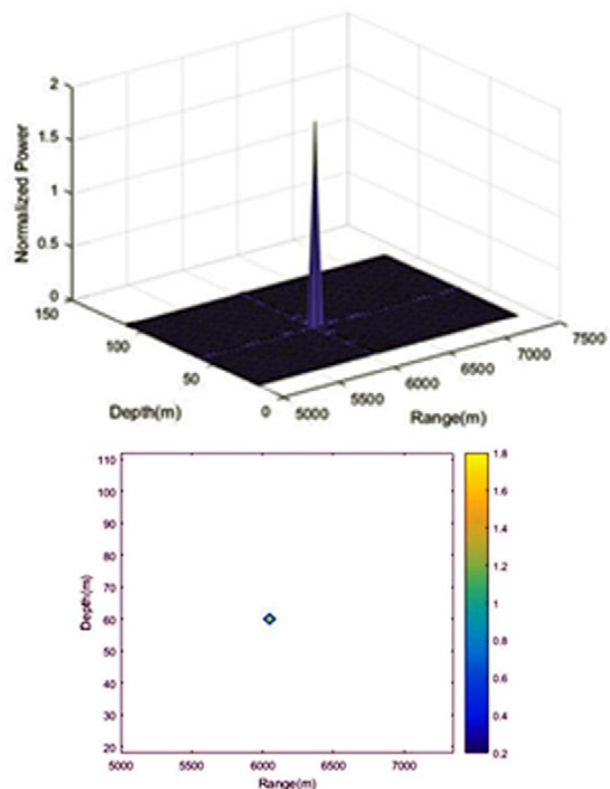
Fig. 4.4 **:** Riemannian ambiguity surface for 20 modeled field replicas and 10 data replicas, SNR=10dB, No of snapshot> 30 samples. The result is reproduced from [5]

Fig. 4.5**:** Riemannian ambiguity surface for 6 modeled replicas and 10 data replicas, SNR=10 dB, No of snapshot>30 samples. The result is reproduced from [5].
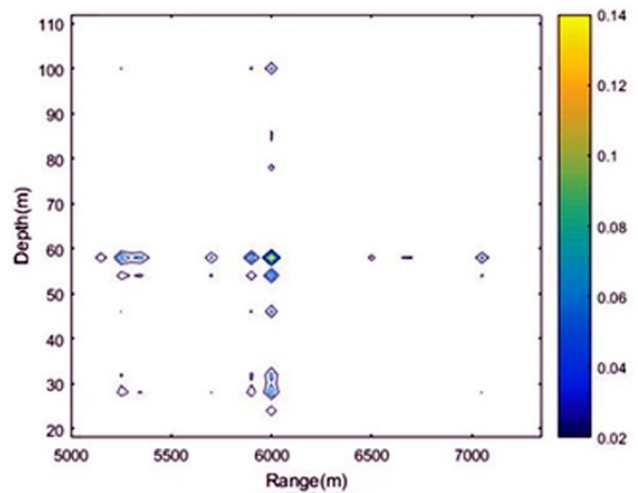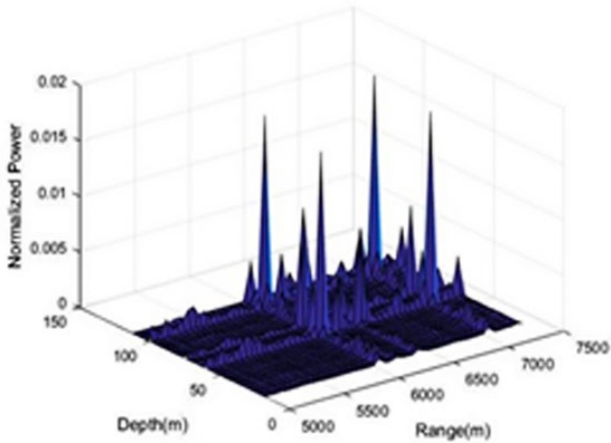
Fig. 4.6: Riemannian ambiguity surface for 3 modeled replicas and 10 data replicas, SNR=10dB, No of snapshot>30 samples. The result is reproduced from [5].
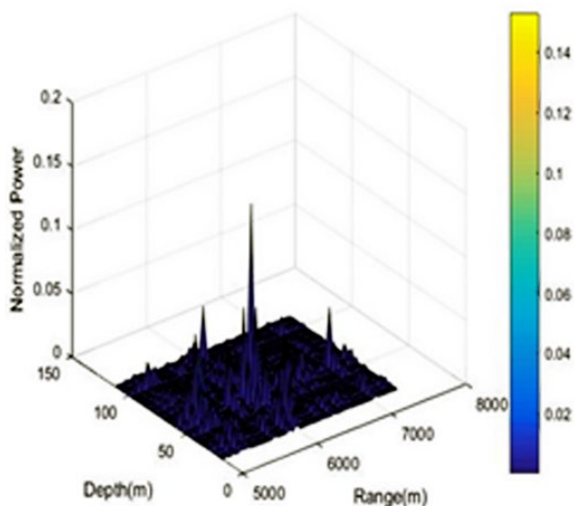
4. 3. 2. Circular Hydrophone Array

The array factor of Circular Hydrophone Array of 32 elements is iso-tropic, symmetrical is depicted in Cartesian coordinate in Fig. 4.7 as follows.
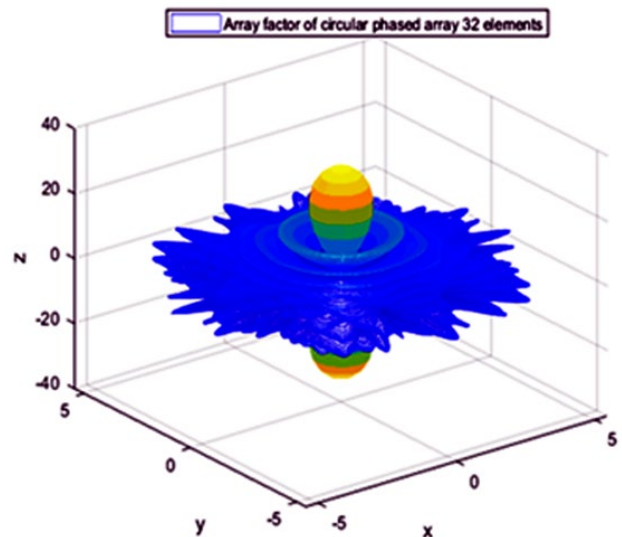
Fig. 4.7 The array factor of Circular Hydrophone Array of 32 elements.

4. 3. 3. Cylindrical Hydrophone Array (CHA)

The geometry of a cylindrical hydrophone array of MxN elements is shown in Cartesian coordinate in Fig. 4.8 as follows
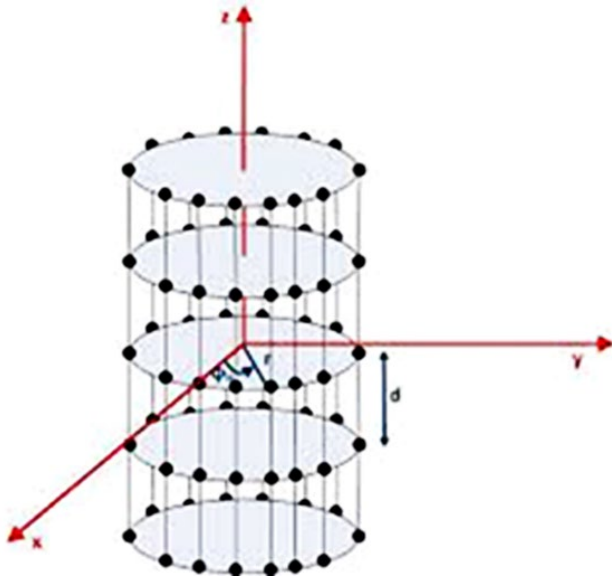
Fig. 4.8. The geometry of cylindrical hydrophone array of MxN elements (each ring has M elements)

When combining 10 rings in Z-axis with each ring spaced by λ/2 (half of wave length) we obtain the cylindrical hydrophone array of 32x10 elements. The array factor of the array is simulated and depicted in Cartesian coordinate as in Fig. 4.9 as follows.
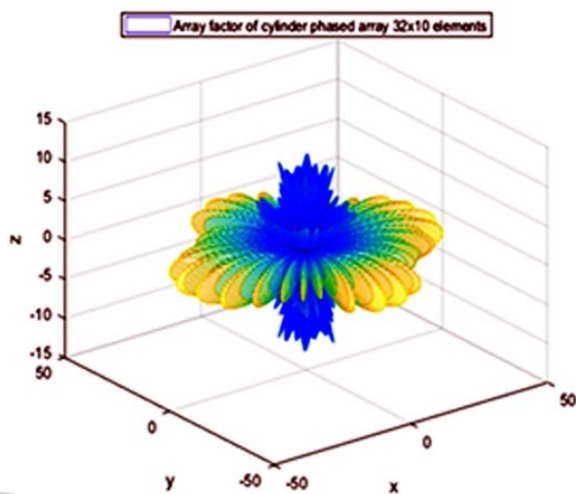
Fig. 4.9 The array factor of cylindrical hydrophone array of 32x10 elements. The result is reproduced from [7]

The range and the depth of the source is estimated with the same results which is obtained using the vertical hydrophone array as in Part 4.3.1.

In addition, the bearing accuracy of circular array is the same form of linear array [7]. So if we use a CHA of 32x10 elements, the bearing accuracy up to $\theta_{opt} \approx \Delta\theta_{3dB}/80 = 9/80 = 0.1^0$
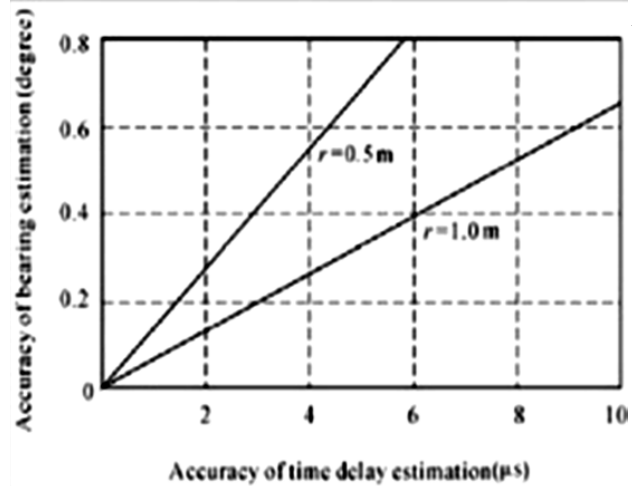
Fig. 4.10 Bearing accuracy of circle hydrophone array (N=64 elements). The result is reproduced from [7].

4. 4. Conclusion

In term of robust signal processing the criteria performance of RMFP is not mean square error of the true source location but the system gain of the robust signal processing. By discussion the capability of RMFP in this chapter we may conclude that it can be adaptively to the mismatch cases more than the conventional MFP. Obviously, with their strong foundation both of MFP and Riemannian Geometry, we believed RMFP will be the future of MFP in the context of lack of acoustic data (It means that we not consider the case of having big acoustic data or exploiting AI applications).

Bibliography

1. http://spib.rice.edu/spib/saclant.html

2. Y. Li, K. M. Wong, Riemannian distances for signal classification by power spectral density. IEEE. J. Sec. Top. Sig. Processing. 7(4), p. 655–669, 2013

3. S. Finette and P. C. Mignerey, Stochastic matched field localization of an acoustic source based on principles of Riemannian geometry, J. Acoustic. Soc. Am 143 (6), p. 3628–3638, 2018

4. R. Cao et al, Passive broad band source localization based on a Riemannian distance with a short vertical array in the deep ocean, J. Acoustic. Soc. Am 145 (6), p. 567–573, June 2019.

5. T. C. Quyen, Matched field processing for source localization based on an approach of Riemannian geometry, AKSUTIKA, Vol.33, pp.71-71, 2019.

6. T. C. Quyen, Stochastic matched field processing using directed Riemannian distance, AKUSTIKA, Vol. 40, pp.2-6, 2021

7. T. C. Quyen, Underwater source localization using cylindrical hydrophone array and Riemannian matched field processing, AKUSTIKA, Vol. 42, pp. 6-12, 2022

Tran Cao Quyen (Ph.D) is the member of Faculty of Electronics and Telecommunications, University of Engineering and Technology, Vietnam National University, Hanoi (VNUH), Vietnam. His major subject consists of Antenna and propagation, RADAR, Underwater Acoustic, and SONAR. Dr. Quyen is the author over 30 technical papers and supervises 2 Ph.D students, 3 master students and dozens of Bachelor in Electronics and Telecommunications.

Over his professional career, he successfully combined academic teaching with practical application of the results of his research. For instance, his product, namely, **OFDM underwater acoustic modem using IC technology** has been received much attention from Vietnam National University as well as Vietnam Navy.

For the problem of underwater source localization, he interested in **Riemannian Matched Field Processing** and suggested to Czech Republic Navy as well as Vietnam Navy using a passive SONAR system which is embedded the proposed algorithms.